Atmos. Chem. Phys. Discuss., https://doi.org/10.5194/acp-2019-46
Manuscript under review for journal Atmos. Chem. Phys.
Discussion started: 3 April 2019

Atmospheric Chemistry and Physics Discussions

Fossil fuel combustion and biomass burning sources of global black carbon

Ling Qi[1] and Shuxiao Wang[1,2]

[1]State Key Joint Laboratory of Environment Simulation and Pollution Control, School of Environment, Tsinghua University, Beijing 100084, China
[2]State Environmental Protection Key Laboratory of Sources and Control of Air Pollution Complex, Beijing 100084, China

Correspondence to: Shuxiao Wang (shxwang@tsinghua.edu.cn)

Abstract. We identify sources (fossil fuel versus biomass burning) of black carbon (BC) in the atmosphere and in deposition using a global 3D chemical transport model GEOS-Chem. We validate the simulated sources against carbon isotope measurements of BC around the globe and find that the model reproduces biomass burning contribution (f_{bb}, %) in various regions within a factor of 2. GEOS-Chem shows that contribution from biomass burning in the Northern Hemisphere (f_{bb}: 34%) is much less than that in the Southern Hemisphere (52%). Specifically, we find comparable contribution from biomass burning and fossil fuel in South Asia, S. America, S. Pacific, Australia and the Antarctic. f_{bb} is the largest in Africa (64%), followed by that in East Asia (40%), Siberia (35%), the Arctic (33%), Canada (31%), the US (25%), and Europe (19%). f_{bb} is higher in summer (59–78%) than in winter (28–32%) in the Arctic, while it is higher in winter (42–58%) and lower in summer (16–42%) over the Himalayan–Tibetan plateau. The seasonal variations of f_{bb} are relatively flat in North America, Europe, and Asia. We find that double biofuel emissions for domestic heating during cold seasons northern than 45°N increases f_{bb} values in the Arctic and Europe in winter by ~30%, resulting in a ~20% reduction of discrepancies of f_{bb} in the two regions. The remaining large negative discrepancies (Europe: 41%; Arctic: 46%) suggest that the biofuel emissions are probably still underestimated at high latitudes. Increasing fraction of thickly coated hydrophilic BC from 20% to 70% in fresh biomass burning plumes increases the fraction of hydrophilic BC in biomass burning plumes by 0–20% (vary with seasons and regions), and thereby reduces atmospheric f_{bb} by up to 11%. Faster aging (4 hour *e*-folding time versus 1.15 days of *e*-folding time) of BC in biomass burning plumes reduces atmospheric f_{bb} by 7% (1– 14%), with the largest reduction in remote regions, such as the Arctic, the Antarctic and S. Pacific. Using size resolved scavenging accelerates scavenging of BC particles in both fossil fuel and biomass burning plumes, with a larger increase of the former. Thus, atmospheric f_{bb} increases in most regions by 1–14%. Overall, atmospheric f_{bb} is determined by f_{bb} in emissions mainly and by atmospheric processes, such as aging and scavenging, to a less extent.

1 Introduction

Black carbon (BC) in the atmosphere and deposited over snow and ice absorbs solar radiation, triggers positive feedbacks and exerts a large positive radiative forcing on the global climate (IPCC, 2014). Estimates of BC radiative forcing span a

large range (0.2–1 W m^{-2}, Bond et al., 2013; IPCC, 2014). One of the uncertainties lies in the orders of magnitude different predictions of BC distributions around the globe, particularly in remote regions, by chemical transport and climate models (Samset et al., 2013; 2014). To reduce the uncertainty, in addition to the widely used BC concentration observations in the troposphere, at surface and in snow, observation-based source apportionment (fossil fuel versus biomass burning) of BC provides another dimension to constrain model simulations of BC distribution. In addition, the optical properties of BC from fossil fuel and biomass burning plumes are distinctively different (Bond et al., 2013), resulting in different radiative forcing from the two sources (Jacobson, 2010). Moreover, because of the relative short lifetime compared to greenhouse gases, accurate source apportionment of BC is important for short-term climate change mitigation. Thus, it is imperative to identify sources of BC globally.

Carbon isotope analysis is effective in separating emissions from fossil fuel combustion (e.g. coal, oil and natural gas) and contemporary biomass burning (expressed as contribution from biomass burning, f_{bb}, %), because fossil emissions are ^{14}C free and biomass emissions have a characteristic $^{14}C/^{12}C$ ratio that is proportional to atmospheric carbon dioxide at the time of carbon fixation (Reddy et al., 2002). Combining $\delta^{13}C$ and $\Delta^{14}C$ measurements further differentiate the contribution from coal and liquid fossil fuel combustion (oil, gasoline and diesel, Andersson et al., 2015 and references therein). Fossil fuel combustion often has an anthropogenic origin, including industrial use, domestic cooking and heating, and transport (Bond et al., 2007). Contemporary biomass burning can from both anthropogenic and natural sources. The former includes mainly industrial and domestic burning of biofuels (fuelwood, charcoal, agricultural residues, and dung, Fernandes et al., 2007) and the latter involves open fires of forests, crops, grass, and peatlands (van der Werf et al., 2010). Carbon isotope measurements are widely used for source apportionment of BC in the atmosphere in South Asia (Gustafsson et al., 2009; Budhavant et al., 2015), East Asia (Chen et al., 2013; Andersson et al., 2015; Zhang et al., 2015; Li et al., 2016), Europe (Szidat et al., 2006; 2009; Zhang et al., 2012) and the Arctic (Barrett et al., 2015; Winiger et al., 2015; 2016; 2017), in snow over the Himalayan-Tibetan Plateau (Li et al., 2016) and in ice core in Alpine (Jenk et al., 2006).

Previous studies (Gustafsson et al., 2009; Chen et al., 2013; Li et al., 2016) compare carbon isotope measurements directly to f_{bb} of local bottom-up emission inventories. The assumption behind this comparison is that the major controlling factor of f_{bb} in the atmosphere is local emissions. However, BC-containing particles in fossil fuel and biomass burning plumes have distinctively different mixing states and hygroscopicities (Moteki et al., 2007; Schwarz et al., 2008; Shiraiwa et al., 2007; Akagi et al., 2012), which might further affect BC scavenging in the two kinds of plumes and thus f_{bb} in the atmosphere and after deposition. Li et al. (2016) found smaller contribution from fossil fuel in snow than in air, suggesting that biomass burning emissions are easier to deposit compared to fossil fuel combustion emissions. Possible factors affecting f_{bb} in the atmosphere and in deposition are mixing states and hygroscopicities in freshly emitted fossil fuel and biomass burning plumes, the following aging rate and scavenging. However, as far as we are aware, no study so far has quantified the contribution of different factors to sources of global BC in the atmosphere and in deposition.

In this study, we simulate sources of BC (fossil fuel combustion versus biomass burning) using a global 3D chemical transport model GEOS-Chem. We describe the model and the carbon isotope measurements in Sections 2 and 3,

Atmos. Chem. Phys. Discuss., https://doi.org/10.5194/acp-2019-46
Manuscript under review for journal Atmos. Chem. Phys.
Discussion started: 3 April 2019

Atmospheric Chemistry and Physics Discussions

respectively. We evaluate the model simulation of f_{bb} in Section 4.1, analyze the spatial and temporal variations of f_{bb} in Section 4.2, evaluate the uncertainties associated with f_{bb} in BC emissions, BC mixing state and hycroscopicity in fresh emissions, aging rage and size-resolved scavenging in Section 4.3.

2 Model description

GEOS-Chem is a global chemical transport model driven with assimilated meteorological fields from the Goddard Earth Observing System (GEOS) of the NASA Global Modeling and Assimilation Office. We use GEOS-Chem v11.01 coupled with the TwO Moment Aerosol Section (TOMAS) microphysics scheme (Adams and Seinfeld, 2002). We use 15 size bins ranging from 3 mn to 10 μm with tracers for sulphate, sea salt, organic aerosols, BC, and dust (Pierce et al., 2007; Lee et al., 2009; D'Andrea et al., 2013; Kodros and Peirce, 2017). MERRA2 meterological data set are used to drive model simulation at 4° latitude × 5° longitude resolution and 47 vertical layers from the surface to 0.01 hPa. Global fossil fuel and biofuel combustion emissions of BC are from Bond et al. (2007) and Fernandes et al. (2007). We replace BC emissions in Asia by Li et al. (2017). We use daily open fire emissions from Global Fire Emissions Database version 4 (GFED4, Giglio et al., 2013) in this study. We assume 20% of the freshly emitted BC aerosols are thickly coated and are hydrophilic (Park et al., 2003). We assume hydrophobic BC is converted to hydrophilic with an *e*-folding time of 1.15 days (Park et al., 2005). Wet deposition follows Liu et al. (2001), with updates in Wang et al. (2011) and Qi et al. (2017a).

GEOS-Chem captures the probability density function (PDF) of annual BC concentrations at sites in the US, Europe, China and the Arctic (see site description in Qi et al., 2017(b)) but overestimates the frequency of low BC concentrations (Fig. 1S (a)). About 30% of the simulated annual BC concentration in air is underestimated by a factor of 2 (Fig. 1S (b)). The model reproduces the PDF of BC concentration in snow preferably (Fig. 2S (a)). The simulated median BC concentrations in snow in various regions agree with observations within a factor of 2, except in region NC_Northest Border (Fig. 2S (b)), where the model overestimates the observed BC concentration in snow by a factor of 3 due to the overestimate of local emissions in that region (Qi et al., 2017b).

3 Observation data

Carbon isotope analysis of BC sources in the atmosphere is available at 41 sites across the globe in different seasons during 2002–2014 (Table S1 and Fig. S3). Generally, f_{bb} values are larger in remote regions (54% in South Asia, 46% in the Arctic and 39% over the Himalayan–Tibetan plateau) than those in urban regions (13% in North America and 29% in East Asia), indicating a larger contribution from biofuel and open fires in rural, developing and remote regions.

Isotope mass balance equation based on the $\Delta^{14}C$ ($^{14}C/^{12}C$) data was applied to apportion the relative contributions to atmospheric BC from biomass burning of modern carbon (f_{bb}) and fossil fuel combustion.

Atmos. Chem. Phys. Discuss., https://doi.org/10.5194/acp-2019-46
Manuscript under review for journal Atmos. Chem. Phys.
Discussion started: 3 April 2019

Atmospheric Chemistry and Physics Discussions

$$\Delta^{14}C = \Delta^{14}C_{bb} f_{bb} + \Delta^{14}C_{ff} (1 - f_{bb})$$

Where $\Delta^{14}C$ is the measured radiocarbon content of the BC component and $\Delta^{14}C_{ff}$ is -1,000‰ by definition because fossil carbon is completely depleted in radiocarbon. $\Delta^{14}C_{bb}$ end member used in this equation is usually between +70 and +225‰, depending on the type and age of the burned biomass. The former value corresponds to freshly produced biomass, such as crop and grass. The latter value reflects the burn of wood, which has accumulated over the decades-to-century-long life span. Different choice of the $\Delta^{14}C_{bb}$ end member is one of the uncertainties associated with this source apportionment method. Uncertainty of ±25‰ translates to < 5% in the resulting f_{bb} estimate (Winiger et al., 2016). Another uncertainty stems from the method of isolating BC from total carbon in sampled particles. Zhang et al. (2012) found that for thermal-optical method, the water-extraction treatment prior to thermal treatment and the heating temperature during thermal treatment are important to the isolation of BC and organic carbon and the following isotope analysis. They found that different protocols of thermal-optical method lead to ~ 30% difference of estimated f_{bb} values.

4 Results and Discussions

4.1 Contribution of biomass burning to BC in various regions

GEOS-Chem simulated f_{bb} in the atmosphere agree with observations within a factor of 2 (Fig.1 (a)). f_{bb} values in Europe and the Arctic are underestimated by a factor of 2, while f_{bb} in North America is overestimated by a factor of 2. The low bias of f_{bb} in Europe occurs in non-summer seasons (observation: 34%, model: 14%), which is partly due to the underestimate of biofuel combustion for domestic heating by current emission inventories in most of the European regions during cold seasons (Herich et al., 2011). The low bias of f_{bb} in the Arctic can also be partly attributed to this underestimate of biofuel, since European emissions are large sources of BC in the Arctic (e.g. Qi et al., 2017c and references therein). Another reason for the low bias of f_{bb} in the Arctic is the underestimate of domestic biofuel usage in Russia as indicated by a recent study (Winiger et al., 2017). In North America, the model overestimates f_{bb} at Salt Lake City and Mexican City by a factor of 2. Possible reasons for the overestimate are explained in Sect. 4.2.1. In E. Asia and S. Asia, the model reproduces the observed f_{bb} values within 10%. In addition, GEOS-Chem underestimates the large variations of f_{bb} values (error bars in Fig. 1 (a)) in the Arctic, Europe, and the Himalayan–Tibetan Plateau, due to the coarse horizontal and vertical resolutions.

Over the Himalayan–Tibetan plateau, observations show that biomass burning dominates BC deposited in snow (64%), but its contribution in the atmosphere is much less (39%). GEOS-Chem reproduces the average f_{bb} in snow perfectly (model: 63%) but overpredicts the average atmospheric f_{bb} (model: 62%) by a factor of 1.6. GEOS-Chem simulated f_{bb} values of BC deposition in snow at all sites over the Himalayan–Tibetan plateau agree with observations within 40% during both monsoon (June–August) and non-monsoon seasons (Fig. 1 (b)), suggesting that the model captures the spatial and temporal variations of f_{bb} in BC deposition in this region. The overestimate of the atmospheric f_{bb} is mainly from the factor of 2.3 overestimate of

f_{bb} during monsoon season (observation: 29%, model: 67%). Possible reasons for the overestimate are discussed in Sect. 4.2.1.

4.2 Temporal and spatial variations of f_{bb} in different regions

4.2.1 Temporal variation of f_{bb}

In the Arctic at Abisko, observed f_{bb} ranges from fall and wintertime low of 31% to summer high of 59% (Fig. 2(a)), due to the large contribution from open fires in Europe in summer (Winiger et al., 2016). The model also shows a peak of f_{bb} in summer, but the seasonal variation is relatively flat (from 23% in winter to 27% in summer). We attribute the discrepancy to two reasons. First, fossil fuel and biofuel emissions (Bond et al., 2007; Fernando et al., 2007) used in this study are annual and lack temporal variations. Second, the coarse resolution does not solve the vortex structure of the low-pressure and frontal systems, which is important for poleward transport of BC (Ma et al., 2014; Sato et al., 2016). Thus, the transport of large open burning emissions in Europe to site Abisko is probably underestimated. At Barrow (Fig. 2 (b)), the seasonal variation of atmospheric f_{bb} is even stronger, from 17% in winter to 78% in summer. The similar magnitudes and variations of f_{bb} in local emissions and the atmosphere in summer at the site suggest that the atmospheric f_{bb} is largely determined by local emissions. In other seasons, the atmospheric f_{bb} values are much larger than the f_{bb} of local emissions, indicating a large contribution from long-range transport.

In contrast to the seasonal cycles of f_{bb} at sites in the Arctic, at Bode (Fig. 2(c)) over the Himalayan–Tibetan Plateau, f_{bb} values are the lowest in summer (17%) and highest in winter (42%). Similar trend is shown at Lumbini (Fig. 2(d)), only with smaller amplitude (summer low: 42%, spring high: 58%). The lower f_{bb} in summer is because of several reasons. First, less biofuel is consumed for domestic heating in warmer seasons (Li et al., 2016). Second, the region is barely affected by open fires. Third, biomass-sourced BC is removed more efficiently by the frequent precipitation in summer both over the Himalayan–Tibetan plateau and over the surrounding source regions, such as India and East Asia (Li et al., 2016). The GEOS-Chem simulated atmospheric f_{bb} of BC at all sites over the Himalayan–Tibetan plateau (results for Bode and Lumbini are shown and the others are not) have weak or no seasonal variations. In addition, the model does not capture the observed increasing trend of f_{bb} along the Mustang valley and Langtang valley. Possible reasons for the discrepancies are several folds. First, the relative contributions of fossil fuel and biofuel emissions in the model have no seasonal cycle. Second, it is conceivable that the coarse model resolution of global models does not reproduce the complex topography and transport pathways of BC over the Himalayan–Tibetan plateau (He et al., 2014). However, the mean modeled atmospheric f_{bb} generally agrees with observations (within 60%) and the modeled atmospheric f_{bb} generally follows the f_{bb} of local emissions across the whole plateau. These comparisons suggest that the atmospheric f_{bb} over the Himalayan–Tibetan plateau is largely determined by f_{bb} in emissions in the region.

In North America (Fig. 2(e)), East Asia (Fig. 2(f)), and South Asia (Fig. 2(g) and (h)), no statistically significant differences of f_{bb} among seasons were observed. However, BC concentrations show strong seasonal variations at the four sites, with high

loadings in winter and low loadings in summer (Mouteva et al., 2017; Yamamoto et al., 2007; Budhavant et al., 2015). In Salt Lake City in North America, the most significant local sources of $PM_{2.5}$ particles are mobile emissions, which are relatively stable through the whole year. The second most important source is area sources with solid fuel burning, which is not allowed to use when air quality forecasts predict an inversion period (Mouteva et al., 2017). This restriction limits the extra use of solid fuels in winter, and thus limited their effects on BC concentrations and f_{bb} in the atmosphere. So the higher concentration of BC in winter in Salt Lake City is largely determined by the low boundary layer height, which is proved to have limited effects on f_{bb} (Mouteva et al., 2017). The model overestimates f_{bb} in all seasons by a factor of 2–4. Modeled f_{bb} in the atmosphere is much higher than the f_{bb} values of local emissions, suggesting a large regional effect on f_{bb} in this region. However, the observations were in urban environment with strong influence from local emissions. This mismatch of model representation and observations partly explains the large positive bias of f_{bb}. In Tokyo, East Asia, the model reproduces both the magnitude and the seasonal variations of observed f_{bb}. The much lower f_{bb} value in emissions than in the atmosphere also indicates a regional effect. In South Asia, GEOS-Chem reproduces the observed seasonal f_{bb} within 30%. Comparison of f_{bb} in local emissions and in the atmosphere suggest that f_{bb} at MCOH is largely affected by long-range transport, while f_{bb} at SINH is mostly affected by local emissions. At MCOH the high f_{bb} is probably from the large f_{bb} in the outflow of Africa, while at SINH local burning of agricultural crop residues are the major sources (Budhavant et al., 2015).

4.2.2 Spatial variation of f_{bb}

The Southern Hemisphere has a higher contribution from biomass burning both for BC in surface air (52%) and in deposition (55%, Fig. 3 (a) and (b)). The high f_{bb} in S. America and Australia are largely from active open fires (accounting for 48% and 81% of the total biomass burning contributions, respectively), while in Africa biofuel consumption is the major biomass burning source (64%, Fig. 3 (c) and (d)). Because of the strong seasonal variations of open fire emissions, the highest f_{bb} in Africa, S. America, S. Pacific, Australia and the Antarctic usually occur during September to November (58–71%), and the lowest values are in March–May (32–56%, Fig. S3).

In the Northern Hemisphere, the largest f_{bb} of both BC in the atmosphere (54%) and in deposition (54%) are in South Asia, where biomass burning contribution dominates over fossil fuel emissions. East Asia has the second largest f_{bb} (41% for BC in air and 43% for BC in deposition) due to large biofuel consumption. In other regions, such as Europe, Canada, the US, Siberia and the Arctic, fossil fuel contribution (65–80%) is much larger than biomass burning. f_{bb} of BC in air and in deposition in different regions have different seasonal variations (Figs. S4–S5). Canada, Siberia, and the Arctic have the strongest seasonal variation with a peak in summer (49–55%) because of the large contribution from open fire emissions (Fig. S6–S7). In the US, Europe, East Asia and South Asia, seasonal variation of f_{bb} is relatively flat, consistent with observations (Fig. 2).

Atmos. Chem. Phys. Discuss., https://doi.org/10.5194/acp-2019-46
Manuscript under review for journal Atmos. Chem. Phys.
Discussion started: 3 April 2019

Atmospheric Chemistry and Physics Discussions

4.3 Uncertainty analysis

4.3.1 Uncertainty associated with biofuel emissions

Biofuel emission estimates are associated with large uncertainties (Fernandes et al., 2007). Source apportionment of BC in Europe based on multi-wavelength aethalometer measurements showed that f_{bb} in winter (24–33%) is much higher than that in summer (2–10%), suggesting that wood burning for domestic heating increases the f_{bb} value in the atmosphere in winter significantly (Herich et al., 2011). In addition, Winiger et al. (2017) analyzed f_{bb} based on carbon isotope measurements at Tiksi in Russia and suggested that domestic wood burning is an important source of BC, emissions of which are underestimated by current bottom-up emission inventories. Thus, we doubled biofuel emissions from domestic heating northern than 45°N during cold seasons in Exp. A. It is conceivable that the largest effects occur in the Northern four regions, including Europe, Siberia, Canada and the Arctic. Specifically, f_{bb} values increase by ~30% in Europe, Siberia and the Arctic and by 15% in Canada in winter, larger than that in spring and fall (4–13%, Fig. 4). Consequently, the model discrepancies of f_{bb} in Europe and the Arctic are reduced from -54% and -56% to -41% and -46%, respectively. This improvement suggests that the biofuel emissions at high latitudes in the Northern Hemisphere are probably too low in current bottom-up BC emission inventories, supporting previous estimates (Herich et al., 2011; Winiger et al., 2017).

4.3.2 Uncertainty associated with hygroscopicity of BC in freshly emitted biomass burning plumes

Recent measurements find that in fossil fuel plumes the fraction of thickly coated hydrophilic BC is ~10% (Moteki et al., 2007; Schwarz et al., 2008; Shiraiwa et al., 2007), while in biomass burning plumes the fraction reaches up to 70% (Schwarz et al., 2008; Akagi et al., 2012). The higher hygroscopicity of BC in freshly emitted biomass burning plumes enhances the subsequent wet scavenging rate and thereby reduces f_{bb} in the atmosphere. We investigate the effects of the initial hygroscopicity of BC in fresh emissions on atmospheric f_{bb} of BC in Exp. B by assuming 70% of freshly emitted BC particles from biomass burning are thickly coated and hydrophilic. The resulting fraction of hydrophilic BC in biomass burning plumes in the 12 regions increase by 0–20% (vary with seasons and regions), lowering f_{bb} in the atmosphere by up to 11%. The largest reduction of f_{bb} shows in June–August (-7%, Fig. 4), when open fires are frequent and active globally (Giglio et al., 2013; van der Werf et al., 2010). During this time, the largest reductions are in Canada (-11%) and Siberia (-10%), where the fraction of hydrophilic BC in biomass burning plumes increases by a large fraction (11–13%). In S. Pacific, the reduction of f_{bb} is large (-10%) as well, because large precipitation over this region removes more biomass burning BC particles in the outflow of S. America. During September–November, reduction of f_{bb} in the Northern Hemisphere (-6%) is much larger than that in the Southern Hemisphere (-1%), because f_{bb} values in the Southern Hemisphere are too large (Fig. S5). The changes of f_{bb} values in other seasons are marginal.

Atmos. Chem. Phys. Discuss., https://doi.org/10.5194/acp-2019-46
Manuscript under review for journal Atmos. Chem. Phys.
Discussion started: 3 April 2019

4.3.3 Uncertainty associated with BC aging time

Mixing with organic and inorganic particles with larger hygroscopicity, BC particles become more hydrophilic during aging process (Bond et al., 2013). It is assumed that BC particles are converted from hydrophobic to hydrophilic with an *e*-folding time of 1.15 days after emission in the standard simulation (Park et al., 2005). However, observations showed that the fraction of thickly coated hydrophilic BC in urban fossil fuel plumes increases linearly with plume age (0.5–2.3% h^{-1}, Moteki et al., 2007; Shiraiwa et al., 2007; Subramanian et al., 2010; McMeeking et al., 2011), while BC aging follows a logarithmic trend with an *e*-folding time of 4 hours in biomass burning plumes (Akagi et al., 2012). The aging rates differ among plumes because of different BC sizes, co-emitted hygroscopic materials and oxidation capacities of the plumes (Bond et al., 2013). Thus, in Exp. C, we assume fossil fuel combustion generated BC ages linearly with a rate of 1% h^{-1}, while BC from biomass burning plumes ages with an *e*-folding time of 4 hours. This means that the fossil fuel plumes age slower than the standard simulation and be scavenged slower, while the biomass burning plumes age much faster and are removed from the atmosphere faster in precipitation. This aging scheme leads to a 0–24% increase of fraction of hydrophilic BC in the atmosphere, which reduces f_{bb} by up to -14%. The largest reduction of f_{bb} is in S. Pacific in fall (MAM) and summer (DJF) in the Southern Hemisphere, followed by the Antarctic (-12%) during MAM and the Arctic (-11%) during SON. The reduction of f_{bb} is larger in remote regions and smaller in source regions, because it takes time for the different aging rates in fossil fuel and biomass burning plumes to affect the hygroscopicities of BC in the two plumes and the subsequent aging rates.

4.3.4 Uncertainty associated with size resolved scavenging

BC particles emitted from biomass burning plumes are usually larger in size and thicker in coating thickness (Schwarz et al., 2008; Sahu et al., 2012), suggesting an easier removal from the atmosphere. Observations show that the mass median diameter of BC particles in biomass burning plumes is 193 nm with a coating thickness of 65 nm, while in fossil fuel plumes, the mass median diameter and coating thickness are 175 nm and 20 nm (Schwarz et al., 2008; Sahu et al., 2012). In addition, because of the different coating materials, hygroscopicities of BC-containing particles in the two kinds of plumes are different as well. The coating materials of BC in urban plumes are dominated by sulfate and followed by nitrate and primary and secondary organics (Shiraiwa et al., 2007), while in biomass burning plumes, the major coating materials are organics (Sahu et al., 2012). For ambient air, characteristic κ values of organics and inorganics are 0.1 (0.01–0.5) and 0.7 (0.5–1.4, Petters and Kreidenweis, 2007; Gunthe et al., 2011 and references therein). Thus, the hygroscopicity and the following wet scavenging of BC particles in fossil fuel and biomass burning plumes are different. In Exp. D, we use the TOMAS microphysics scheme to process the aging and wet scavenging of BC with different sizes from fossil fuel combustion and biomass burning. The mass median diameters of fossil fuel and biomass burning BC particles are assumed to be 160 nm and 200 nm, respectively. Size resolved coagulation, condensation, nucleation and cloud processing are implemented. Coating materials included are sulfate, nitrate, sea-salt, organics and mineral dust. The size-resolved aging and scavenging scheme leads to a larger increase of fraction of hydrophilic BC in fossil fuel plumes (by 16% (0–31%, vary with regions)) than in

biomass burning plumes (by 12% (0–23%)), suggesting that fossil fuel BC particles are removed faster. Thus atmospheric f_{bb} increases in most regions during MAM (by 1–14%), SON (by 0–7%) and DJF (by 1–12%). The most noticeable characteristics is that the increase of f_{bb} in Northern Hemisphere is larger than those in Southern Hemisphere, due to the large fraction of fossil fuel emissions in the Northern Hemisphere.

5 Conclusions

This study sought to understand the relative contribution of fossil fuel combustion and biomass burning to global BC. We used GEOS-Chem (version 11-01-01) driven by MERRA2 assimilated meteorological fields to simulate BC concentration from fossil fuel and biomass burning. The source apportionment results were expressed as the fraction of BC from biomass burning (f_{bb}). Simulated f_{bb} was validated against carbon isotope measurements of BC in the atmosphere at 41 stations across the Northern Hemisphere and 11 snow samples over the Himalayan–Tibetan plateau. We also investigated the uncertainties of f_{bb} associated with biofuel emissions, fraction of hydrophilic BC in fresh emissions, aging time and size-resolved scavenging.

The model reproduced the mean observed atmospheric f_{bb} in various regions and in snow over the Himalayan–Tibetan plateau within a factor of 2. Generally, values of atmospheric f_{bb} were larger in remote regions (54% in South Asia, 46% in the Arctic and 39% over the Himalayan–Tibetan plateau) than those in urban regions (13% in North America and 29% in East Asia), indicating a larger contribution from biofuel and open burning sources in rural, developing and remote regions. f_{bb} was higher in summer (59–78%) than in winter (28–32%) in the Arctic, while it was higher in winter (42–58%) and lower in summer (16–42%) over the Himalayan–Tibetan plateau. The simulated amplitudes of the seasonal variations were much smaller in the two regions. The seasonal variation was observed to be relatively flat in North America, Europe, East and South Asia. The model reproduced the monthly mean f_{bb} in these regions within 30%. The Southern Hemisphere had a higher atmospheric f_{bb} than the Northern Hemisphere (SH: 52%, NH: 34%) due to the large fraction of open burning emissions in S. America and Australia and large fraction of biofuel consumption in Africa. In the Northern Hemisphere, the highest f_{bb} was in South Asia (54%), followed by East Asia (41%), due to large biofuel consumption. In other regions, such as Europe, Canada, the US, Siberia and the Arctic, f_{bb} values are small (20–35%).

Simulated f_{bb} was associated with uncertainties from all processes, including emissions, aging and deposition. We found that doubled biofuel emissions used for domestic heating northern than 45°N resulted in a ~30% increase of f_{bb} in Europe, Siberia and the Arctic and a 15% increase in Canada in winter. This increase reduced the discrepancy of f_{bb} against observations by 18–23%, suggesting that the biofuel emissions at high latitudes were underestimated by the bottom-up emission inventories. Using a higher fraction of hydrophilic BC in fresh biomass burning plumes (uncertainty simulation: 70%, standard simulation: 20%) resulted in a reduction of f_{bb} in summer by -2 – -11%, with the largest reduction in Canada and Siberia, where open fires were frequent. In the standard simulation, it was assumed that BC in both fossil fuel and biomass burning plumes aged following an *e*-folding time of 1.15 days. In the uncertainty simulation, we used a 4 hour *e*-folding life time for

BC in biomass burning plumes and a linear aging rate of 1% for BC in fossil fuel plumes. This leaded to a reduction of f_{bb} up to -14% in the atmosphere. The largest reduction was in S. Pacific in fall (MAM) and summer (DJF) in the Southern Hemisphere. The reductions in the Antarctic (-12%) and the Arctic (-11%) were also large in fall when there were large open fires in the Southern Hemisphere and at high latitudes in the Northern Hemisphere. Size-resolved aging and scavenging scheme leaded to a larger increase of fraction of hydrophilic BC in fossil fuel plumes (by 16% (0–31%)) than in biomass burning plumes (by 12% (0–23%)). Thus atmospheric f_{bb} increased in most regions during MAM (by 1–14%), SON (by 0–7%) and DJF (by 1–12%).

Previous studies (Healy et al., 2015 and references therein) showed that internally mixed BC from open fires in Quebec has no optical lensing effect. Considering the large contribution from biomass burning in S. Asia and in the Southern Hemisphere, the inclusion of lensing-related absorption enhancement in climate models for BC from all sources may lead to an overestimate of the radiative forcing. Measurements of the optical properties of BC particles from different sources in different regions are needed to better constrain BC radiative forcing.

Author contribution

Ling Qi and Shuxiao Wang designed the experiments. Ling Qi performed the simulations. Ling Qi prepared the manuscript with contributions from Shuxiao Wang.

Acknowledgments

This work was supported by the National Natural Science Foundation of China (21625701) and National research program for key issues in air pollution control (DQGG0301).

References

Adams, P. J., and Seinfeld, J. H.: Predicting global aerosol size distributions in general circulation models, Journal of Geophysical Research: Atmospheres, 107(D19), 4370-4392, doi:10.1029/2001JD001010, 2002.

Akagi, S. K., Craven, J. S., Taylor, J. W., McMeeking, G. R., Yokelson, R. J., Burling, I. R., Urbanski, S. P., Wold, C. E., Seinfeld, J. H., Coe, H., Alvarado, M. J., and Weise, D. R.: Evolution of trace gases and particles emitted by a chaparral fire in California, Atmospheric Chemistry and Physics, 12, 1397-1421, doi:10.5194/acp-12-1397-2012, 2012.

Andersson, A., Deng, J., Du, K., Zheng, M., Yan, C., Skold, M., and Gustafsson, O.: Regionally-varying combustion sources of the January 2013 severe haze events over eastern China, Environ Sci Technol, 49, 2038-2043, doi:10.1021/es503855e, 2015.

Barrett, T. E., Robinson, E. M., Usenko, S., and Sheesley, R. J.: Source Contributions to Wintertime Elemental and Organic Carbon in the Western Arctic Based on Radiocarbon and Tracer Apportionment, Environ Sci Technol, 49, 11631-11639, doi:10.1021/acs.est.5b03081, 2015.

Bond, T. C., Bhardwaj, E., Dong, R., Jogani, R., Jung, S., Roden, C., Streets, D. G., and Trautmann, N. M.: Historical emissions of black and organic carbon aerosol from energy-related combustion, 1850-2000, Global Biogeochemical Cycles, 21, GB2018, doi:10.1029/2006gb002840, 2007.

Bond, T. C., Doherty, S. J., Fahey, D. W., Forster, P. M., Berntsen, T., DeAngelo, B. J., Flanner, M. G., Ghan, S., Kärcher, B., Koch, D., Kinne, S., Kondo, Y., Quinn, P. K., Sarofim, M. C., Schultz, M. G., Schulz, M., Venkataraman, C., Zhang, H., Zhang, S., Bellouin, N., Guttikunda, S. K., Hopke, P. K., Jacobson, M. Z., Kaiser, J. W., Klimont, Z., Lohmann, U., Schwarz, J. P., Shindell, D., Storelvmo, T., Warren, S. G., and Zender, C. S.: Bounding the role of black carbon in the climate system: A scientific assessment, Journal of Geophysical Research: Atmospheres, 118, 5380-5552, doi:10.1002/jgrd.50171, 2013.

Budhavant, K., Andersson, A., Bosch, C., Kruså, M., Kirillova, E. N., Sheesley, R. J., Safai, P. D., Rao, P. S. P., and Gustafsson, Ö.: Radiocarbon-based source apportionment of elemental carbon aerosols at two South Asian receptor observatories over a full annual cycle, Environmental Research Letters, 10, 064004, doi:10.1088/1748-9326/10/6/064004, 2015.

Chen, B., Andersson, A., Lee, M., Kirillova, E. N., Xiao, Q., Krusa, M., Shi, M., Hu, K., Lu, Z., Streets, D. G., Du, K., and Gustafsson, O.: Source forensics of black carbon aerosols from China, Environ Sci Technol, 47, 9102-9108, doi:10.1021/es401599r, 2013.

D'Andrea, S., Häkkinen, S., Westervelt, D., Kuang, C., Levin, E., Kanawade, V., Leaitch, W., Spracklen, D., Riipinen, I., and Pierce, J.: Understanding global secondary organic aerosol amount and size-resolved condensational behavior, Atmospheric Chemistry and Physics, 13(22), 11519-11534, doi: 10.5194/acp-13-11519-2013, 2013.

Fernandes, S. D., Trautmann, N. M., Streets, D. G., Roden, C. A., and Bond, T. C.: Global biofuel use, 1850-2000, Global Biogeochemical Cycles, 21(2), GB2019, doi:10.1029/2006gb002836, 2007.

Giglio, L., Randerson, J. T., and van der Werf, G. R.: Analysis of daily, monthly, and annual burned area using the fourth-generation global fire emissions database (GFED4), Journal of Geophysical Research: Biogeosciences, 118(1), 317-328, doi:10.1002/jgrg.20042, 2013.

Gunthe, S. S., Rose, D., Su, H., Garland, R. M., Achtert, P., Nowak, A., Wiedensohler, A., Kuwata, M., Takegawa, N., Kondo, Y., Hu, M., Shao, M., Zhu, T., Andreae, M. O., and Pöschl, U.: Cloud condensation nuclei (CCN) from fresh and aged air pollution in the megacity region of Beijing, Atmospheric Chemistry and Physics, 11, 11023-11039, doi:10.5194/acp-11-11023-2011, 2011.

Gustafsson, Ö., Kruså, M., Zencak, Z., Sheesley, R. J., Granat, L., Engström, E., Praveen, P., Rao, P., Leck, C., and Rodhe, H.: Brown clouds over South Asia: biomass or fossil fuel combustion?, Science, 323, 495-498, doi: 10.1126/science.1164857, 2009.

He, C., Li, Q. B., Liou, K. N., Zhang, J., Qi, L., Mao, Y., Gao, M., Lu, Z., Streets, D. G., Zhang, Q., Sarin, M. M., and Ram, K.: A global 3-D CTM evaluation of black carbon in the Tibetan Plateau, Atmospheric Chemistry and Physics, 14, 7091-7112, doi:10.5194/acp-14-7091-2014, 2014.

Herich, H., Hueglin, C., and Buchmann, B.: A 2.5 year's source apportionment study of black carbon from wood burning and fossil fuel combustion at urban and rural sites in Switzerland, Atmospheric Measurement Techniques, 4, 1409-1420, doi:10.5194/amt-4-1409-2011, 2011.

IPCC: Climate Change 2014: Synthesis Report. Contribution of Working Groups I, II and III to the Fifth Assessment Report of the Intergovernmental Panel on Climate Change, edited by: Core Writing Team, Pachauri, R. K. and Meyer, L. A., IPCC, Geneva, Switzerland, 151 pp, 2014.

Jacobson, M. Z.: Short-term effects of controlling fossil-fuel soot, biofuel soot and gases, and methane on climate, Arctic ice, and air pollution health, Journal of Geophysical Research, 115, D14209, doi:10.1029/2009jd013795, 2010.

Jenk, T., Szidat, S., Schwikowski, M., Gäggeler, H., Brütsch, S., Wacker, L., Synal, H.-A., and Saurer, M.: Radiocarbon analysis in an Alpine ice core: record of anthropogenic and biogenic contributions to carbonaceous aerosols in the past (1650–1940), Atmospheric chemistry and physics, 6, 5381-5390, doi: 10.5194/acp-6-5381-2006, 2006.

Kodros, J., and Pierce, J.: Important global and regional differences in aerosol cloud‐albedo effect estimates between simulations with and without prognostic aerosol microphysics, Journal of Geophysical Research: Atmospheres, 122, 4003-4018, doi: 10.1002/2016JD025886, 2017.

Lee, Y., Chen, K., and Adams, P.: Development of a global model of mineral dust aerosol microphysics, Atmospheric Chemistry and Physics, 9, 2441-2458, doi: 10.5194/acp-9-2441-2009, 2009.

Li, C., Bosch, C., Kang, S., Andersson, A., Chen, P., Zhang, Q., Cong, Z., Chen, B., Qin, D., and Gustafsson, O.: Sources of black carbon to the Himalayan-Tibetan Plateau glaciers, Nat Commun, 7, 12574, doi: 10.1038/ncomms12574, 2016.

Li, M., Zhang, Q., Kurokawa, J.-i., Woo, J.-H., He, K., Lu, Z., Ohara, T., Song, Y., Streets, D. G., Carmichael, G. R., Cheng, Y., Hong, C., Huo, H., Jiang, X., Kang, S., Liu, F., Su, H., and Zheng, B.: MIX: a mosaic Asian anthropogenic emission inventory under the international collaboration framework of the MICS-Asia and HTAP, Atmospheric Chemistry and Physics, 17, 935-963, doi:10.5194/acp-17-935-2017, 2017.

Liu, H., Jacob, D. J., Bey, I., and Yantosca, R. M.: Constraints from 210Pb and 7Be on wet deposition and transport in a global three‐dimensional chemical tracer model driven by assimilated meteorological fields, Journal of Geophysical Research: Atmospheres, 106, 12109-12128, doi: 0148-0227/01/2000 JD900839, 2001.

Ma, P.-L., Rasch, P. J., Fast, J. D., Easter, R. C., Gustafson Jr, W., Liu, X., Ghan, S. J., and Singh, B.: Assessing the CAM5 physics suite in the WRF-Chem model: Implementation, resolution sensitivity, and a first evaluation for a regional case study, Geoscientific Model Development Discussion, 7, 755, doi:10.5194/gmd-7-755-2014, 2014.

McMeeking, G. R., Morgan, W. T., Flynn, M., Highwood, E. J., Turnbull, K., Haywood, J., and Coe, H.: Black carbon aerosol mixing state, organic aerosols and aerosol optical properties over the United Kingdom, Atmospheric Chemistry and Physics, 11, 9037-9052, doi:10.5194/acp-11-9037-2011, 2011.

Moteki, N., Kondo, Y., Miyazaki, Y., Takegawa, N., Komazaki, Y., Kurata, G., Shirai, T., Blake, D. R., Miyakawa, T., and Koike, M.: Evolution of mixing state of black carbon particles: Aircraft measurements over the western Pacific in March 2004, Geophysical Research Letters, 34, L11803, doi:10.1029/2006gl028943, 2007.

Mouteva, G. O., Randerson, J. T., Fahrni, S. M., Bush, S. E., Ehleringer, J. R., Xu, X., Santos, G. M., Kuprov, R., Schichtel, B. A., and Czimczik, C. I.: Using radiocarbon to constrain black and organic carbon aerosol sources in Salt Lake City, Journal of Geophysical Research: Atmospheres, 122, 9843-9857, doi:10.1002/2017jd026519, 2017.

Park, R. J., Jacob, D. J., Chin, M., and Martin, R. V.: Sources of carbonaceous aerosols over the United States and implications for natural visibility, Journal of Geophysical Research: Atmospheres, 108, 4355, doi: 10.1029/2002jd003190, 2003.

Park, R. J., Jacob, D. J., Palmer, P. I., Clarke, A. D., Weber, R. J., Zondlo, M. A., Eisele, F. L., Bandy, A. R., Thornton, D. C., and Sachse, G. W.: Export efficiency of black carbon aerosol in continental outflow: Global implications, Journal of Geophysical Research: Atmospheres, 110, D11205, doi: 10.1029/2004jd005432, 2005.

Petters, M., and Kreidenweis, S.: A single parameter representation of hygroscopic growth and cloud condensation nucleus activity, Atmospheric Chemistry and Physics, 7, 1961-1971, doi: 10.5194/acp-7-1961-2007, 2007.

Pierce, J., Chen, K., and Adams, P.: Contribution of primary carbonaceous aerosol to cloud condensation nuclei: processes and uncertainties evaluated with a global aerosol microphysics model, Atmospheric Chemistry and Physics, 7, 5447-5466, doi: 10.5194/acp-7-5447-2007, 2007.

Qi, L., Li, Q., He, C., Wang, X., and Huang, J.: Effects of the Wegener–Bergeron–Findeisen process on global black carbon distribution, Atmospheric Chemistry and Physics, 17, 7459-7479, doi:10.5194/acp-17-7459-2017, 2017a.

Qi, L., Li, Q., Henze, D. K., Tseng, H.-L., and He, C.: Sources of springtime surface black carbon in the Arctic: an adjoint analysis for April 2008, Atmospheric Chemistry and Physics, 17, 9697-9716, doi:10.5194/acp-17-9697-2017, 2017b.

Qi, L., Li, Q., Li, Y., and He, C.: Factors controlling black carbon distribution in the Arctic, Atmospheric Chemistry and Physics, 17, 1037-1059, doi:10.5194/acp-17-1037-2017, 2017c.

Reddy, C. M., Pearson, A., Xu, L., McNichol, A. P., Benner, B. A., Wise, S. A., Klouda, G. A., Currie, L. A., and Eglinton, T. I.: Radiocarbon as a tool to apportion the sources of polycyclic aromatic hydrocarbons and black carbon in environmental samples, Environmental Science & Technology, 36, 1774-1782, doi: 10.1021/es011343f , 2002.

Sahu, L. K., Kondo, Y., Moteki, N., Takegawa, N., Zhao, Y., Cubison, M. J., Jimenez, J. L., Vay, S., Diskin, G. S., Wisthaler, A., Mikoviny, T., Huey, L. G., Weinheimer, A. J., and Knapp, D. J.: Emission characteristics of black carbon in anthropogenic and biomass burning plumes over California during ARCTAS-CARB 2008, Journal of Geophysical Research: Atmospheres, 117, D16302, doi:10.1029/2011jd017401, 2012.

Samset, B. H., Myhre, G., Schulz, M., Balkanski, Y., Bauer, S., Berntsen, T. K., Bian, H., Bellouin, N., Diehl, T., Easter, R. C., Ghan, S. J., Iversen, T., Kinne, S., Kirkevåg, A., Lamarque, J. F., Lin, G., Liu, X., Penner, J. E., Seland, Ø., Skeie, R. B., Stier, P., Takemura, T., Tsigaridis, K., and Zhang, K.: Black carbon vertical profiles strongly affect its radiative forcing uncertainty, Atmospheric Chemistry and Physics, 13, 2423-2434, doi:10.5194/acp-13-2423-2013, 2013.

Samset, B. H., Myhre, G., Herber, A., Kondo, Y., Li, S. M., Moteki, N., Koike, M., Oshima, N., Schwarz, J. P., Balkanski, Y., Bauer, S. E., Bellouin, N., Berntsen, T. K., Bian, H., Chin, M., Diehl, T., Easter, R. C., Ghan, S. J., Iversen, T., Kirkevåg, A., Lamarque, J. F., Lin, G., Liu, X., Penner, J. E., Schulz, M., Seland, Ø., Skeie, R. B., Stier, P., Takemura, T., Tsigaridis, K., and Zhang, K.: Modelled black carbon radiative forcing and atmospheric lifetime in AeroCom Phase II constrained by aircraft observations, Atmospheric Chemistry and Physics, 14, 12465-12477, doi:10.5194/acp-14-12465-2014, 2014.

Sato, Y., Miura, H., Yashiro, H., Goto, D., Takemura, T., Tomita, H., and Nakajima, T.: Unrealistically pristine air in the Arctic produced by current global scale models, Scientific reports, 6, 26561, doi:10.1038/srep26561, 2016.

Schwarz, J. P., Gao, R. S., Spackman, J. R., Watts, L. A., Thomson, D. S., Fahey, D. W., Ryerson, T. B., Peischl, J., Holloway, J. S., Trainer, M., Frost, G. J., Baynard, T., Lack, D. A., de Gouw, J. A., Warneke, C., and Del Negro, L. A.: Measurement of the mixing state, mass, and optical size of individual black carbon particles in urban and biomass burning emissions, Geophysical Research Letters, 35, L13810, doi:10.1029/2008gl033968, 2008.

Shiraiwa, M., Kondo, Y., Moteki, N., Takegawa, N., Miyazaki, Y., and Blake, D. R.: Evolution of mixing state of black carbon in polluted air from Tokyo, Geophysical Research Letters, 34, L16803, doi:10.1029/2007gl029819, 2007.

Subramanian, R., Kok, G., Baumgardner, D., Clarke, A., Shinozuka, Y., Campos, T., Heizer, C., Stephens, B., De Foy, B., and Voss, P. B.: Black carbon over Mexico: the effect of atmospheric transport on mixing state, mass absorption cross-section, and BC/CO ratios, Atmospheric Chemistry & Physics, 10, 219-237, doi:10.5194/acp-10-219-2010, 2010.

Szidat, S., Jenk, T. M., Synal, H.-A., Kalberer, M., Wacker, L., Hajdas, I., Kasper-Giebl, A., and Baltensperger, U.: Contributions of fossil fuel, biomass-burning, and biogenic emissions to carbonaceous aerosols in Zurich as traced by14C, Journal of Geophysical Research, 111, doi:10.1029/2005jd006590, 2006.

Szidat, S., Ruff, M., Perron, N., Wacker, L., Synal, H.-A., Hallquist, M., Shannigrahi, A. S., Yttri, K. E., Dye, C., and Simpson, D.: Fossil and non-fossil sources of organic carbon (OC) and elemental carbon (EC) in Göteborg, Sweden, Atmospheric Chemistry and Physics, 9, 1521-1535, doi: 10.5194/acp-9-1521-2009, 2009.

van der Werf, G. R., Randerson, J. T., Giglio, L., Collatz, G. J., Mu, M., Kasibhatla, P. S., Morton, D. C., DeFries, R. S., Jin, Y., and van Leeuwen, T. T.: Global fire emissions and the contribution of deforestation, savanna, forest, agricultural, and peat fires (1997–2009), Atmospheric Chemistry and Physics, 10, 11707-11735, doi:10.5194/acp-10-11707-2010, 2010.

Wang, Q., Jacob, D. J., Fisher, J. A., Mao, J., Leibensperger, E. M., Carouge, C. C., Le Sager, P., Kondo, Y., Jimenez, J. L., Cubison, M. J., and Doherty, S. J.: Sources of carbonaceous aerosols and deposited black carbon in the Arctic in winter-spring: implications for radiative forcing, Atmospheric Chemistry and Physics, 11, 12453-12473, doi:10.5194/acp-11-12453-2011, 2011.

Winiger, P., Andersson, A., Yttri, K. E., Tunved, P., and Gustafsson, O.: Isotope-Based Source Apportionment of EC Aerosol Particles during Winter High-Pollution Events at the Zeppelin Observatory, Svalbard, Environ Sci Technol, 49, 11959-11966, doi:10.1021/acs.est.5b02644, 2015.

Winiger, P., Andersson, A., Eckhardt, S., Stohl, A., and Gustafsson, Ö.: The sources of atmospheric black carbon at a European gateway to the Arctic, Nature Communications, 7, 12776, doi:10.1038/ncomms12776, 2016.

Winiger, P., Andersson, A., Eckhardt, S., Stohl, A., Semiletov, I. P., Dudarev, O. V., Charkin, A., Shakhova, N., Klimont, Z., Heyes, C., and Gustafsson, O.: Siberian Arctic black carbon sources constrained by model and observation, Proc Natl Acad Sci U S A, 114, E1054-E1061, doi:10.1073/pnas.1613401114, 2017.

Yamamoto, N., Muramoto, A., Yoshinaga, J., Shibata, K., Endo, M., Endo, O., Hirabayashi, M., Tanabe, K., Goto, S., and Yoneda, M.: Comparison of carbonaceous aerosols in Tokyo before and after implementation of diesel exhaust restrictions, Environmental science & technology, 41, 6357-6362, doi:10.1021/acs.est.5b02644, 2007.

Zhang, Y. L., Perron, N., Ciobanu, V. G., Zotter, P., Minguillón, M. C., Wacker, L., Prévôt, A. S. H., Baltensperger, U., and Szidat, S.: On the isolation of OC and EC and the optimal strategy of radiocarbon-based source apportionment of carbonaceous aerosols, Atmospheric Chemistry and Physics, 12, 10841-10856, doi:10.5194/acp-12-10841-2012, 2012.

Zhang, Y. L., Huang, R. J., El Haddad, I., Ho, K. F., Cao, J. J., Han, Y., Zotter, P., Bozzetti, C., Daellenbach, K. R., Canonaco, F., Slowik, J. G., Salazar, G., Schwikowski, M., Schnelle-Kreis, J., Abbaszade, G., Zimmermann, R., Baltensperger, U., Prévôt, A. S. H., and Szidat, S.: Fossil vs. non-fossil sources of fine carbonaceous aerosols in four Chinese cities during the extreme winter haze episode of 2013, Atmospheric Chemistry and Physics, 15, 1299-1312, doi:10.5194/acp-15-1299-2015, 2015.

Atmos. Chem. Phys. Discuss., https://doi.org/10.5194/acp-2019-46
Manuscript under review for journal Atmos. Chem. Phys.
Discussion started: 3 April 2019

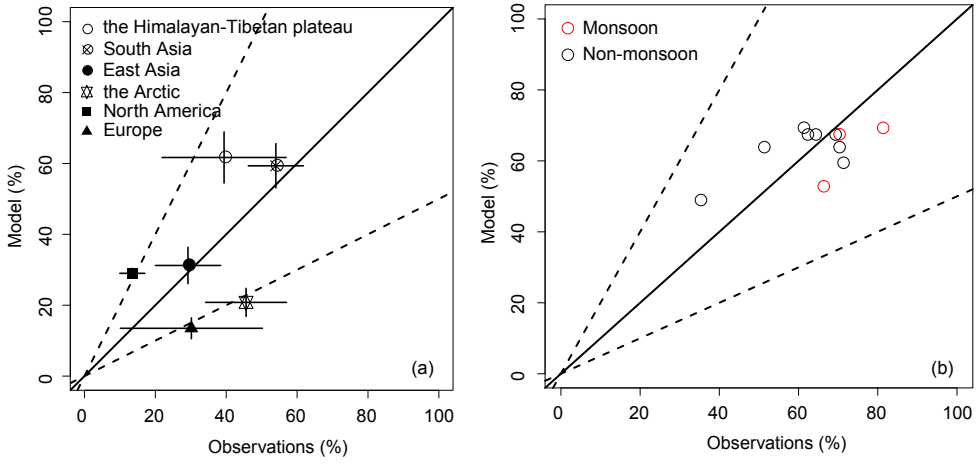

Figure 1: Observed and GEOS-Chem simulated fraction of biomass burning (f_{bb}, %) of (a) BC in the atmosphere in the Arctic, South Asia, North America, Europe, East Asia, and the Himalayan-Tibetan plateau (the regions are symbol-coded) and (b) BC in snow during monsoon (red) and non-monsoon (black) seasons over the Himalayan-Tibetan plateau. Also shown in (a) are the standard deviations of observed and model simulated f_{bb} in each region (error bars). Observations of f_{bb} in the atmosphere in (a) are from carbon isotope analysis as listed in Table S1. Observations of f_{bb} in BC in snow in (b) are from Li et al. (2016). Solid lines in (a) and (b) are 1:1 ratio lines and dashed lines are 1:2 (or 2:1).

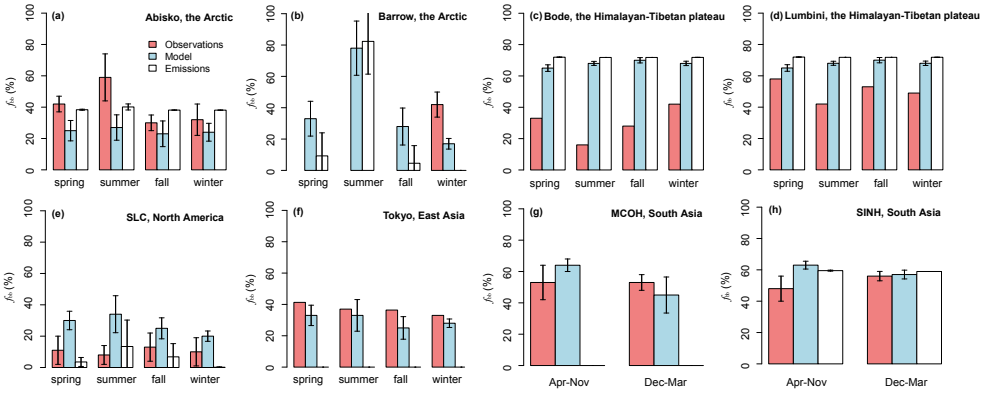

Figure 2: Seasonal variations of observed (lightcoral bars) and GEOS-Chem simulated (lightblue bars) f_{bb} of BC in the atmosphere at (a) Abisko and (b) Barrow in the Arctic, (c) Bode and (d) Lumbini over the Himalayan–Tibetan Plateau, (e) Salt Lake City in North America, (f) Tokyo in East Asia, (g) MCOH and (h) SINH in South Asia. The white bars are f_{bb} values of BC emissions in the model grid of each site. Also shown are the standard deviations (error bars). Site locations are shown in Fig. S3.

Atmos. Chem. Phys. Discuss., https://doi.org/10.5194/acp-2019-46
Manuscript under review for journal Atmos. Chem. Phys.
Discussion started: 3 April 2019

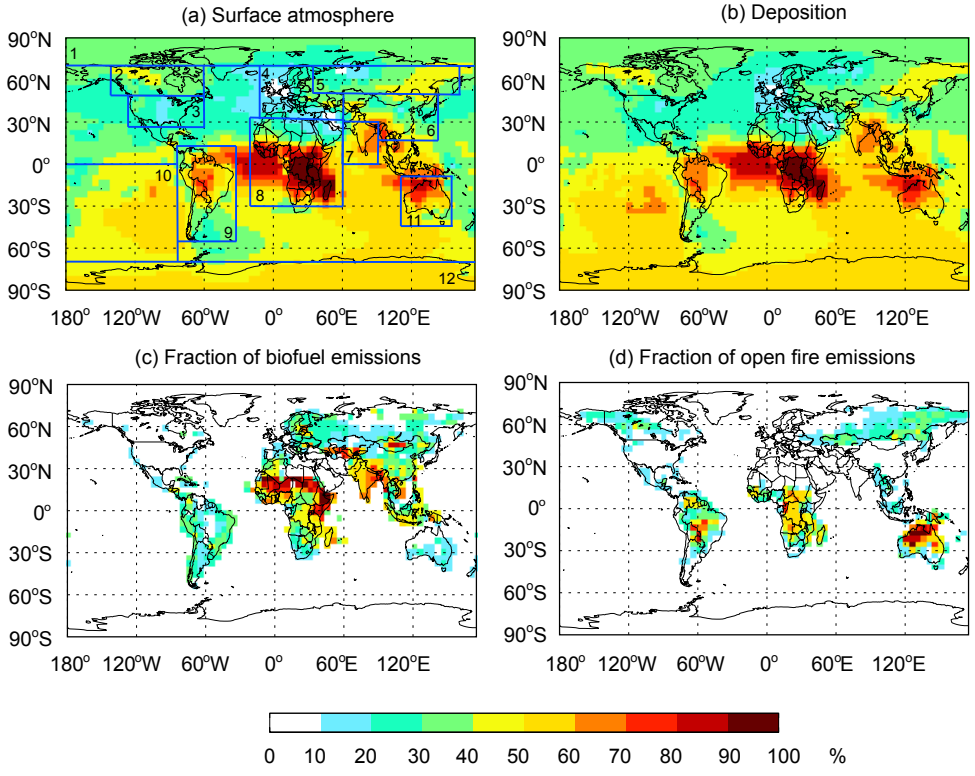

Figure 3: Annual (a) f_{bb} of BC in the atmosphere at surface, (b) f_{bb} of BC deposition, (c) fraction of biofuel emissions and (d) fraction of open fire emissions. Data are averaged for 2007–2013. Also shown in (a) are regions discussed in the text: 1. the Arctic, 2. Canada, 3. the US, 4. Europe, 5. Siberia, 6. E. Asia, 7. S. Asia, 8. Africa, 9. S. America, 10. S. Pacific, 11. Australia, and 12. the Antarctic.

Atmos. Chem. Phys. Discuss., https://doi.org/10.5194/acp-2019-46
Manuscript under review for journal Atmos. Chem. Phys.
Discussion started: 3 April 2019

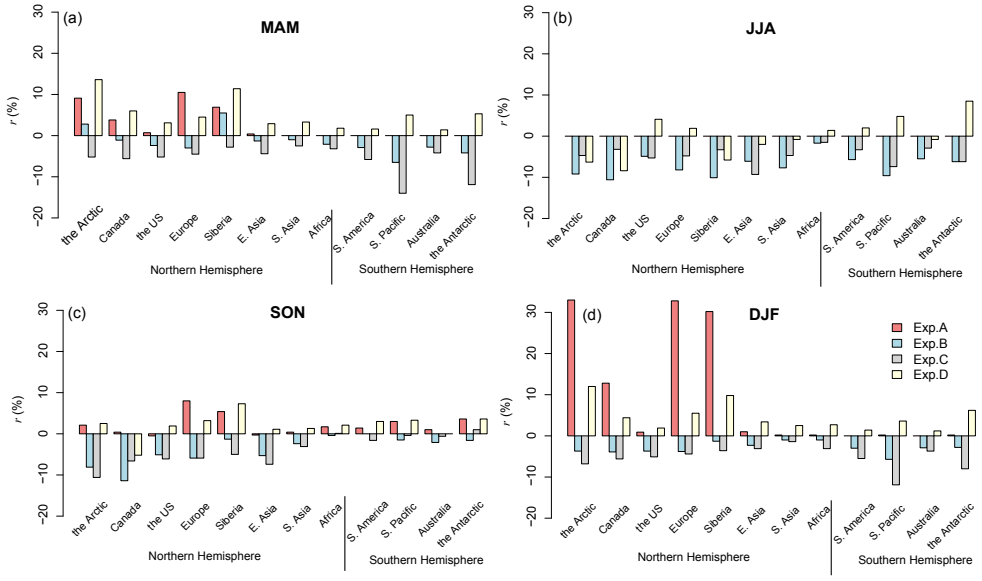

Figure 4: GEOS-Chem simulated fractional change (*r*) to atmospheric f_{bb} relative to the standard simulation, as a result of doubled biofuel emissions northern than 45°N (Exp. A), 70% of hydrophilic BC of freshly emitted biomass burning BC-containing particles (Exp. B), 4 hour *e*-folding aging time of BC in biomass burning plumes and linear aging rate of 1% in fossil fuel plumes (Exp. C) and TOMAS microphysical aging and scavenging (Exp. D), $r = ([BC]_{Exp.} - [BC]_{Std.})/[BC]_{Std.}$, that varies with regions (see region definition in Fig.3 (a)) and seasons ((a) March–May (MAM), (b) June–August (JJA), (c) September–November (SON) and (d) December–February (DJF)), averaged for 2007–2013. See details of the standard simulation and the uncertainty experiments in the text.